[^{11}C]Choline Positron Emission Tomography in Estrogen Receptor–Positive Breast Cancer

Kaiyumars B. Contractor,[1] Laura M. Kenny,[1] Justin Stebbing,[1] Adil Al-Nahhas,[2] Carlo Palmieri,[1] Dudley Sinnett,[3] Jacqueline S. Lewis,[3] Katy Hogben,[3] Safiye Osman,[5] Sami Shousha,[4] Charles Lowdell,[1] R. Charles Coombes,[1] and Eric O. Aboagye[1]

Abstract

Purpose: Novel radiotracers could potentially allow the identification of clinically aggressive tumor phenotypes. As choline metabolism increases during malignant transformation and progression of human mammary epithelial cells, we examined the ability of [^{11}C]choline (CHO) positron emission tomography imaging to detect clinically aggressive phenotype in patients with estrogen receptor (ER)–positive breast cancer *in vivo*.

Experimental Design: CHO positron emission tomography was done in 32 individuals with primary or metastatic ER–positive breast cancer. Semiquantitative (standardized uptake value) and fully quantitative (net irreversible transfer rate constant of CHO, Ki) estimates of CHO uptake in the tumors were calculated and compared with tumor grade, size, involved nodes, and also ER, progesterone receptor, Ki-67, and human epidermal growth factor receptor-2 scores.

Results: Breast tumors were well visualized in 30 of 32 patients with good tumor background ratios. A wide range of uptake values were observed in primary and metastatic tumors. CHO uptake variables correlated well with tumor grade. For most imaging variables, a poor association was found with tumor size, ER, progesterone receptor, human epidermal growth factor receptor-2, Ki-67, and nodal status.

Conclusions: CHO showed good uptake in most breast cancers and merits further investigation as a breast cancer imaging agent. (Clin Cancer Res 2009;15(17):5503–10)

Breast cancer is the commonest female malignancy with >1.2 million women diagnosed each year worldwide. Over 75% of breast carcinomas express estrogen receptor (ER). Hence, ER-positive breast cancer is usually treated with antiestrogens, such as tamoxifen. Adjuvant hormonal treatment with tamoxifen followed by an aromatase inhibitor for a total of 5 years (1), as well as aromatase inhibitors alone (2), have been shown to improve recurrence-free survival and overall survival. However, patients relapse despite adjuvant hormonal therapy, due to drug resistance. Only approximately half of the patients with recurrence in ER-positive disease respond to endocrine therapy, whereas the remainder show resistance, clinically evidenced by progression (3). The mechanisms underlying this process are complex, but it is generally agreed that, at least in some patients, cross-talk between cell surface receptor kinases and ER may play a role. In this regard, phosphorylation of ERα by the mitogen-activated protein kinase (MAPK; refs. 4–7) and phosphatidylinositol-3-kinase pathways (3) have been implicated. In particular, MAPK-mediated hyperphosphorylation of ERα on S118, S104, and S106 collectively leads to ligand-independent receptor activation, thereby potentially contributing to resistance to antiendocrine agents, such as tamoxifen and aromatase inhibitors (4, 8, 9). A large proportion of breast cancers have elevated MAPK (10), and expression correlates to poor response to endocrine therapies (11). There is an unmet need to develop imaging methods to guide clinicians as to the correct choice of subsequent therapies.

Whereas FDG positron emission tomography (PET) has been extensively used as an imaging biomarker for diagnosis (12) and for monitoring of treatment response in cancer patients (13), newer imaging biomarkers including [^{18}F]fluorothymidine and [^{11}C]choline (CHO) are being examined for their greater specificity in the assessment of proliferation (14, 15) and choline metabolic activity (16), respectively. The utility of CHO PET in breast cancer has not been studied. Of interest, Aboagye and Bhujwalla (17) previously showed a

Authors' Affiliations: [1]Department of Oncology, Imperial College; [2]Department of Nuclear Medicine, Imperial College Healthcare NHS Trust, Hammersmith Hospital; [3]Department of Breast Surgery and [4]Department of Cellular Pathology, Imperial College Healthcare NHS Trust, Charing Cross Hospital; [5]GE-Imanet, Hammersmith Hospital, London, United Kingdom

Received 3/17/09; revised 5/8/09; accepted 5/28/09; published OnlineFirst 8/25/09.

Grant support: United Kingdom Medical Research Council grant U1200.02.005.00001.01, Cancer Research UK grant C37/A5610, and Experimental Cancer Medicine Centre grant C37/A7283.

The costs of publication of this article were defrayed in part by the payment of page charges. This article must therefore be hereby marked *advertisement* in accordance with 18 U.S.C. Section 1734 solely to indicate this fact.

Requests for reprints: Eric O. Aboagye, Imperial College School of Medicine, Room 240, MRC Cyclotron Building, Clinical Sciences Centre, Hammersmith Hospital, Du Cane Road, London W12 0NN, United Kingdom. Phone: 44-20-8383-3759; Fax: 44-20-8383-1783; E-mail: eric.aboagye@imperial.ac.uk.

doi:10.1158/1078-0432.CCR-09-0666

Translational Relevance

The formation of phosphocholine from choline has been found to increase with malignant transformation and progression of mammary epithelial cells *in vitro*. We therefore hypothesized that, in human tumors, choline metabolism will increase with increasing tumor grade — a measure of progression. In this manuscript we report, for the first time, [^{11}C]choline (CHO) positron emission tomography (PET) imaging of patients with breast cancer. In this patient population, we found that imaging variables derived from the PET scan were associated with tumor grade, reflecting tumor aggressiveness. We conclude from our findings that CHO PET merits further investigation as a PET imaging agent in breast cancer.

unique phenotype of increased choline metabolism in the transition of normal human mammary epithelial cells to immortalized, oncogene-transformed, and finally nonmetastatic and metastatic cancer. In their study, they showed a switch from predominantly higher intracellular metabolite levels of glycerophosphophocholine (degradation pathway) to predominantly higher phosphocholine levels (biosynthetic pathway) early in cell transformation (17). Phosphocholine levels then increased in a stepwise manner with progression (17) such that breast cancer cells had the highest phosphocholine levels. Further studies in mammary epithelial cells showed that the aberrant increases in phosphocholine metabolite levels were due to expression of the biosynthetic enzyme, choline kinase-α (18, 19). Coincidentally, choline kinase activity and cellular phosphocholine levels are regulated by the growth factor receptor–MAPK pathway in mammalian cells (17, 20–24), the same pathway that modulates estrogen-independent growth. Beyond breast cancer, the level of choline kinase-α in tumors of patients with non–small cell lung cancer has been shown recently to have a significant effect on survival; in that study, tumor choline kinase-α expression of at least 1.91 times of that expressed in normal tissue fared worse with respect to relapse-free and lung cancer–specific overall survival after definitive lung cancer surgery (25).

To investigate this further, in the context of the detection of clinically aggressive breast phenotype, we examined the role of CHO PET as an imaging tool in breast cancer. Given that choline metabolism increases with transformation and progression, we hypothesized that high CHO phosphorylation will be associated with high tumor grade, reflecting a more aggressive phenotype.

Materials and Methods

Patients and statistics. Patients with biopsy-proved and ER-positive breast cancer were recruited. We selected this patient population to retain a level of homogeneity with respect to tumor presentation, prognosis, and survival. Recruitment period was for 3.5 y. In this initial study, both primary and heavily pretreated metastatic cases (including lung and omental metastasis and Krukenburg tumors) were included to provide a dynamic range of uptake values. Primary cases were scanned before any treatment. Metastatic cases were those who were progressing in spite of previous therapy in the form of chemotherapy or hormonal therapy and had a chemotherapy-free and radiotherapy-free interval of a minimum of 3 and 4 wk, respectively, before undergoing PET to negate any residual effects of previous therapies. To minimize the effect of partial volume averaging, all individuals scanned required at least one measurable lesion (≥20 mm in the longest dimension), which was confirmed on routine ultrasound (primary cases) or contrast-enhanced spiral computed tomography (metastatic cases). Breast tumors often metastasize to the liver. Tumors in this organ were, however, excluded from analysis because of the high physiologic uptake of CHO (although protocols are under way within our group to overcome this difficulty). Other inclusion criteria were as follows: life expectancy of ≥3 mo, hemoglobin of ≥10 g/dL, granulocyte count of $\geq 1.5 \times 10^9$/L, platelet count of at least 100×10^9/L, adequate creatinine clearance (≥50 mL/min calculated), adequate hepatic function (bilirubin, ≤1.5 upper limit of normal; serum transaminases, ≤2.5 upper limit of normal), and ability to consent and comply fully with the study protocol. The exclusion criteria were pregnant or lactating patients, sexually active patients who were not using adequate contraception (pregnancy tests were done in all women of childbearing potential), patients with uncontrolled medical conditions, patients unable to lie flat, and patients with evidence of cerebral metastases. The study followed the "Declaration of Helsinki's — Ethical Principles for Medical Research involving Human Subjects." Appropriate ethical permission from the Hospital Research Ethics Committee and a license from the Administration of Radioactive Substances Advisory Committee UK were obtained, and all patients provided written informed consent. A minimum of 10 d between core biopsy and PET scanning was ensured to prevent false-positive uptake of CHO.

PET imaging. CHO was manufactured by standard methods at the local hospital as previously described (26, 27). The mean injected activity of CHO measured 320 MBq (range 188-360 MBq) with mean specific radioactivity of 13,279 MBq/μmol and mean radiochemical purity of >99%. PET scanning was done on an ECAT HR+/962 PET scanner (CTI/Siemens) at Hammersmith Hospital with a 15.7-cm field of view.

An arterial cannula was inserted in the radial artery (size 22 G) to allow for continuous (total 50 mL; 5 mL/min) and discrete (total 100 mL; baseline and 2.5, 3.5, 5, 7.5, 10, 15, 20, 30, 45, and 50 min after injection of CHO) blood sampling throughout the CHO scan. A venous cannula (size 22 G) was positioned in the opposite arm for radiotracer injection. The patient was positioned in the scanner with the region of interest centered in the field of view. Single-bed position dynamic PET scanning was commenced 30 s before i.v. injection of CHO as a single bolus and consisted of 26 frames of varying time intervals (5 × 10, 2 × 20, 2 × 30, 5 × 60, 3 × 120, 2 × 180, 3 × 300, and 3 × 600 s) lasting 65 min. Continuous arterial sampling was commenced at the start of the first frame for 10 min. Radioactivity from both continuous and discrete blood and plasma was assessed by gamma counting. Reverse-phase high-performance liquid chromatography with radiochemical detection was used to analyze the proportion of parent CHO and metabolite, [^{11}C]betaine, in the discrete samples. The "arterial input function" necessary for calculation of the kinetic variables of CHO uptake was derived as the plasma parent fraction.

Correction factors were applied to image data for attenuation, scattered radiation, electronic dead time, and random coincidences. Filtered back projection images were used for analysis. Regions of interest were drawn manually around tumor and normal tissues (normal breast and normal lung) using the Analyze software (Biomedical Imaging Resource, Mayo Foundation). The PET analysis was done in an unblinded manner (by K.C.). Semiquantitative analysis was done, and kinetic parameters were derived using Matlab (version 6.0, The Mathworks, Inc.) and in-house software. Standardized uptake values (SUV; ref. 28) were derived from decay-corrected time activity curves (at midframe time periods for each frame) and normalized for injected activity and body surface area (body surface area = $0.20247 \times \text{height (m)}^{0.725} \times \text{weight (kg)}^{0.425}$; University of Wisconsin).[6] Specifically, we derived

[6] http://www.intmed.mcw.edu/clincalc/body.html

Table 1. Patient and tumor characteristics of primary (A) and metastatic (B) cases undergoing CHO PET

A

Patient	Region of tumor	Size	Grade	ER score	PR score	HER-2 score	Involved nodes	$SUV_{av,60} \times 10^{-5}$ (m^2/mL)	$SUV_{max,60} \times 10^{-5}$ (m^2/mL)	$SUV_{av,5-15} \times 10^{-5}$ (m^2/mL)	Ki × 10^{-4} (mL plasma/ mL tissue/s)
1	Breast	29	3	3	1	0	1*	9.2	17.5	9.7	12.7
2	Breast	28	2	3	3	0	0	6.4	9.3	6.6	8.9
3	Breast	37	2	3	3	0		9.9	18.6	10.6	13.5
4	Breast	50	3	3	3	0	0	9.0	22.6	10.2	14.7
5	Breast	30	2	3	2	0	2*	5.4	8.9	6.8	7.8
6	Breast†	25	2				0				
7	Breast	38	2	1	1	0	0	5.6	8.3	6.9	5.5
8	Breast	22	2	3	0	3	1	10.4	14.9	10.7	10.7
	Axillary node	20	2					6.3	9.9	6.7	7.9
9	Breast	20	2	3	0	0	0	5.2	10.1	5.9	7.0
10	Breast	24	1	3	3	0	0	2.1	4.8	2.7	2.1
11	Breast	30	3	3	3	0	1	9.6	18.8	9.3	11.1
	Axillary node	20	3					6.9	11.8	6.4	8.5
12	Breast	38	3	3	0	0	3*	7.1	14.6	8.0	7.5
	Axillary node	22	3					8.1	16.4	8.7	9.2

B

Patient	Region of tumor	Size (mm)	Grade	$SUV_{av,60} \times 10^{-5}$ (m^2/mL)	$SUV_{max,60} \times 10^{-5}$ (m^2/mL)	$SUV_{av,5-15} \times 10^{-5}$ (m^2/mL)	Ki × 10^{-4} (mL plasma/ mL tissue/s)
13	Chest wall	72	2	4.5	7.8	4.9	6.3
	Axillary mass	60	2	12.4	18.1	12.1	17.8
14	Omental mass	60	2	9.4	20.7	10.0	12.8
	Omental mass	60	2	8.0	23.5	7.2	10.7
15	Axillary mass	25	2	6.9	11.0	8.8	11.3
16	Axillary mass	25	2	5.4	9.6	4.3	5.9
17	Neck node	40	3	9.9	15.3	9.3	13.7
	Neck node	38	3	8.8	20.8	8.6	12.3
18	Neck node	25	2	3.8	12.6	5.8	3.4
19	Neck node	20	2	10.6	8.9	11.3	16.7
20	Krukenburg	40	2	4.8	12.4	6.3	7.4
	Krukenburg	40	2	5.6	14.1	6.8	7.2
21	Chest wall mass	58	3	22.6	31.8	21.6	29.9
	Chest wall mass	40	3	17.0	25.3	16.6	22.0
	Mediastinal mass	20	3	12.9	21.3	13.2	16.9
	Mediastinal mass	20	3	13.6	22.5	14.8	17.4
22	Lung†	20	3				
23	Breast	50	3	15.0	24.8	13.8	29.1
	Breast	50	3	14.5	23.7	13.2	27.0
	Axillary mass	25	3	9.9	17.1	9.8	18.4
	Axillary mass	25	3	10.2	17.8	9.6	17.6
	Axillary mass	40	3	13.9	20.3	13.3	25.4
24	Breast	37	3	14.1	18.8	14.4	14.0
25	Breast	40	2	12.3	20.1	12.2	17.6
26	Breast	47	3	6.0	11.4	7.1	12.1
27	Axillary mass	20	3	4.1	6.1	4.7	8.4
28	Breast	46	2	5.5	11.8	5.5	5.7
29	Chest wall	34	2	9.8	15.5	9.8	12.9
30	Lung	25	2	12.9	23.7	13.1	18.2
31	Lung	24	3	10.4	19.0	10.1	15.1
32	Chest wall mass	31	3	8.1	19.8	8.6	18.0

*Patient 1 had a single 10-mm involved axillary node, and patient 5 had two involved axillary nodes, 8 mm and 5 mm, none of which were visible on CHO PET. Patient 12 had two other involved axillary nodes of size <20 mm and not seen on PET.
†Tumor not visualized on PET scan.

semiquantitative measures of CHO uptake including the average uptake at 5 to 15 min ($SUV_{5-15,av}$), the average uptake at 60 min ($SUV_{60,av}$), and the maximal voxel uptake at 60 min ($SUV_{60,max}$). The early and late time frames were selected to reflect transport and phosphorylation (with minimal metabolism) on one hand and retention of radioactivity on the other. In other tumor types, CHO is rapidly taken up by tumor within 5 to 10 min of injection and remains in steady-state up to 40 to 60 min after injection (16, 29).

A modified version of Patlak's (Graphical) analysis described previously for [^{18}F]fluorothymidine (14) and thymidine imaging (30) was

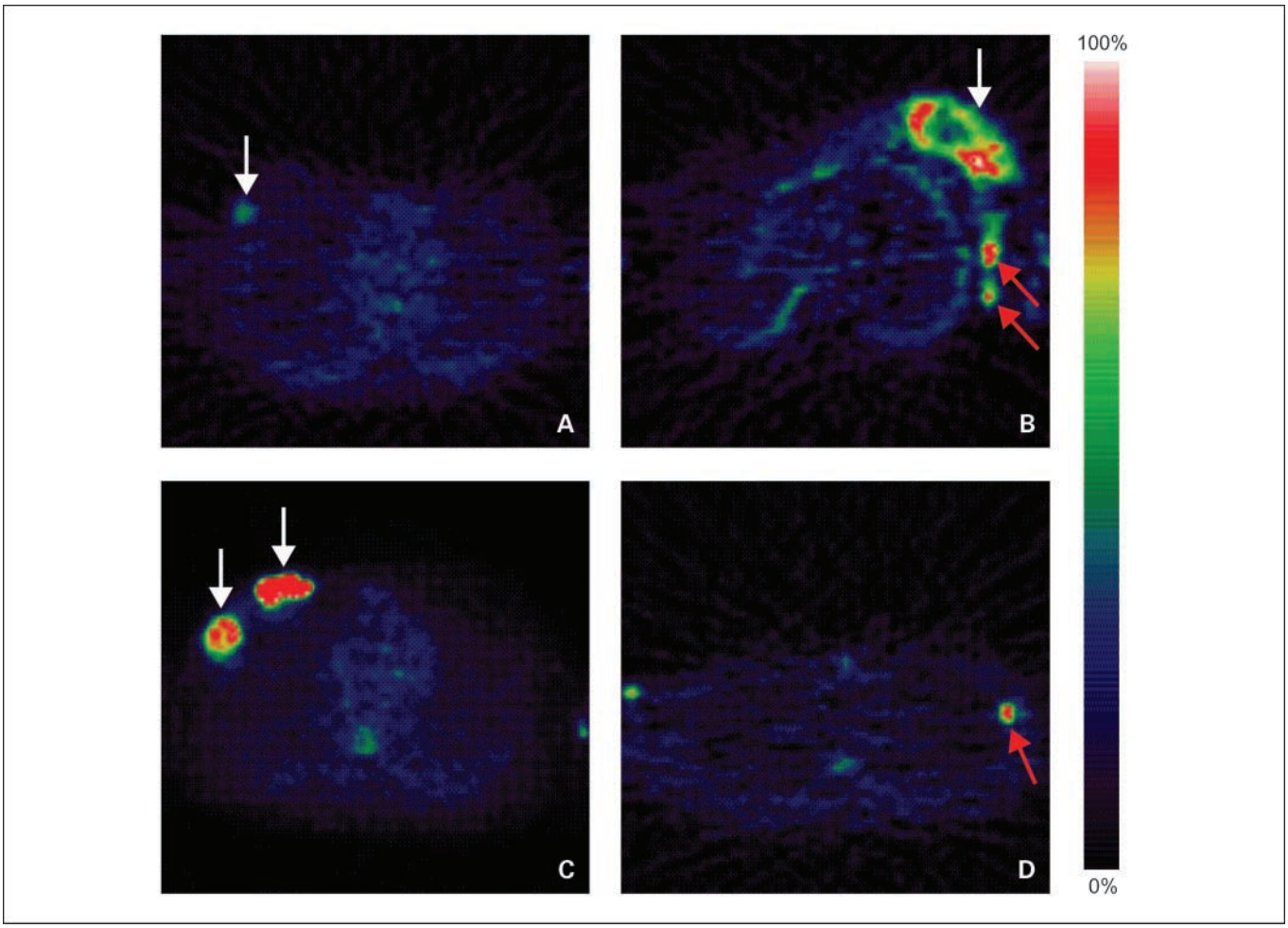

Fig. 1. Transverse CHO PET image of primary ductal carcinoma of the right breast (*A*), large inflammatory ductal carcinoma of the left breast with involved axillary lymph nodes (*B*), and metastatic ductal breast cancer involving the right chest wall (*C*). *D,* primary breast cancer patient showing involved left axillary node (confirmed positive pathologically). White arrows, main tumor; red arrows, secondary deposits in axilla. Note intensity bar.

used to derive the rate constant for the net irreversible uptake of CHO from blood to form phosphocholine in tissue (Ki). The original Patlak technique (31) allows estimation of blood-to-tissue transfer constants from multiple time uptake data. This method is valid if there are no metabolites. If the parent tracer is significantly metabolized, as in the case of CHO to [^{11}C]betaine, then a correction factor is needed to exclude the contribution of metabolites in the exchangeable tissue space. This modification was used to derive Ki for CHO in tumor tissue as follows:

$$\frac{A}{C_{\mathrm{Tot}}} = K_x \frac{\int C_x \delta\tau}{C_{\mathrm{Tot}}} + V$$

wherein V is

$$V = V_{\mathrm{ox}} \frac{C_x}{C_{\mathrm{Tot}}} + \sum V_{\mathrm{om}} \frac{C_m}{C_{\mathrm{Tot}}} + V_v$$

A is total tissue radioactivity (kBq/mL), K_x is Ki for CHO (mL plasma/s/mL tissue), C_{Tot} is total blood radioactivity (kBq/mL), C_x is radioactivity of parent compound determined by radio-high-performance liquid chromatography (kBq/mL), C_m is the radioactivity of metabolite (kBq/mL), τ is the elapsed time from time $t = 0$ (s), V_{ox} is steady-state space of exchangeable region occupied by parent, V_{om} is steady-state space of exchangeable region occupied by the metabolite, and V_b is blood volume. We compared the kinetic and semiquantitative variables of CHO in breast tumors. Tumor PET uptake variables were also compared with that in normal tissues.

Histopathology. We compared each tumor uptake variable to histologic grade as a measure of tumor aggressiveness, ER, progesterone receptor (PR), human epidermal growth factor receptor-2 (HER-2), and the number of involved axillary nodes (primary patients only). Tumor tissue was fixed in formalin and embedded in paraffin wax. Then 4-μm thick sections were cut with a microtome and stained with H&E. Grading of tumor was done using Elston and Ellis's grading system (32). ER and PR scores were graded using the McCarty's H-scoring system (33): 1+, weakly positive; 2+, moderately positive; 3+, strongly positive. The 4B5 (Rabbit Monoclonal Primary Antibody, Ventana Medical Systems, Benchmark XT System) antibody was used for HER-2 immunostaining, and scores were 0 (no staining), 1+ (faint membrane staining in >10% cells), 2+ (weak circumferential staining in >10% cells), and 3+ (strong and thick membrane staining). A positive HER-2 result was a score of either 2+ confirmed positive on fluorescence *in situ* hybridization or 3+. Anti–Ki-67 antibody, NCL-Ki-67-MM1 (Novocastra Laboratories), was used to stain primary tumor biopsies. The numbers of total and Ki-67–positive cells were then manually counted in eight randomly selected fields of view using a BX51 Olympus microscope (Olympus Optical) at ×400 magnification. In patients with metastatic disease, the original grade from their primary tumors was used for comparison with CHO uptake variables. It is well recognized that although expression of markers such as ER, PR, HER-2, and epidermal growth factor receptor

Table 2. Comparison of PET variables with histologic grade and tumor size

	$SUV_{5\text{-}15,av}$		$SUV_{60,max}$		$SUV_{60,av}$		Ki	
	P	*r*	*P*	*r*	*P*	*r*	*P*	*r*
Tumor grade (all cases)	0.0051	0.41	0.0006	0.49	0.0015	0.46	0.0002	0.53
Tumor grade (primary cases)	0.2	0.38	0.005	0.70	0.06	0.51	0.06	0.51
Tumor size (mm)	0.2	0.18	0.02	0.36	0.3	0.16	0.2	0.2
ER score	0.8	0.04	0.8	-0.05	0.9	-0.02	0.4	-0.13
PR score	NP	NP	0.7	0.13	NP	NP	0.3	0.34
HER-2 status	NP	NP	NP	NP	NP	NP	NP	NP
No. involved nodes	0.13	-0.78	0.13	-0.78	0.13	-0.78	0.08	-0.89
Ki-67 score	0.4	0.33	0.4	0.29	0.3	0.36	0.6	0.18

Abbreviations: *r*, Spearman's correlation coefficient; NP, correlation not possible using Spearman's correlation test.

may alter, the grade of breast tumors does not change in the transition from primary to metastasis (34). The comparisons of PET variables with histology were done on a lesion-by-lesion basis. Pathology reports were reviewed by a single, independent pathologist (S.S.).

Statistical analysis. The association between the PET variables and tumor grade, size, ER, PR, HER-2, Ki-67, and number of involved axillary nodes of primary cases was determined by Spearman's correlation test using GraphPad Prism (version 4.00 for Windows, GraphPad Software). The significance level was set at 5%, two-sided tests. *P* values of ≤0.05 were reported as significant.

Results

Characteristics of the subjects and tumor visualization. A total of 32 patients were recruited (12 primary untreated, 20 metastatic) as described in Table 1. Their mean age was 52 years (range, 33-72) and the median tumor size imaged was 34 mm (range, 20-72). Tumor was not visualized in one lobular primary (patient 6) and one case with lung metastasis (patient 22). All other primary and metastatic tumors were visualized with good tumor-background ratios (Fig. 1A-D). Five primary patients (Table 1A) had pathologically involved nodes of which CHO PET detected three lesions correctly (patients 8, 11, and 12). Of the remaining two patients in whom PET failed to detect involved nodes, one (patient 1) had a single 10-mm involved node and the other (patient 5) had two nodes (both <8 mm in diameter). In patients with nodal disease, regions of interest were drawn around visible nodes in the axilla. In these patients, CHO uptake values were in general higher in the primary tumor than in involved axillary nodes, except in patient 12, in whom the metastatic axillary node had a marginally higher uptake (Table 1A); this was not a function of tumor size.

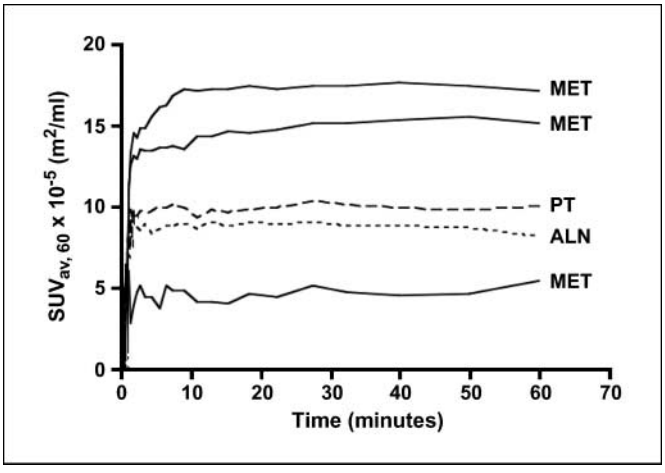

Fig. 2. Time-activity curves of tumors showing uptake with time. PT, primary tumor; ALN, axillary lymph node of primary patient; MET, metastatic tumor.

Two patients scanned (Table 1B) presented with *de novo* metastasis (patient 24 who had liver metastasis and patient 25 who had bone metastasis); the metastases were not assessed by PET scanning. Patient 23 (Fig. 1B) had a large inflammatory carcinoma involving the entire breast with metastasis in the axilla and bone. Other patients with metastases had been heavily pretreated with chemotherapy, hormonal theraphy, and/or radiotherapy but were still progressing. All metastatic lesions found on computed tomography were identified on PET except patient 22 whose basal lung metastasis was not visible on CHO PET. In total, 31 lesions (Table 1) were present in 20 metastatic patients, and thus, all analyses are on a per tumor basis. In three metastatic patients (patients 13, 21, and 23), relatively large differences in CHO PET uptake variables were seen between different tumors in the same patient. Two metastatic patients had biopsies of the metastasis taken just before PET (patients 13 and 15) and the grade matched that of the corresponding primary tumor.

CHO pharmacokinetics in breast tumors was characterized by a very rapid delivery such that steady-state was reached for all tumors within 5 to 10 minutes (within 1 minute for low uptake tumors). Within the bounds of experimental error, including patient movement, radioactivity levels then remained relatively constant for the duration of the scan. Typical examples of time-versus-radioactivity curves are shown in Fig. 2. Semiquantitative and kinetic variables were derived for tumor regions of interest (Fig. 3A and B). The median $SUV_{60,av}$ was 9.1×10^{-5} m^2/mL (range, 2.1-22.6); median $SUV_{5\text{-}15}$ was 9.3×10^{-5} m^2/mL (range, 2.7-21.6); median $SUV_{60,max}$ 16.8×10^{-5} m^2/mL (range, 4.8-31.7); and median Ki was 12.5×10^{-4} mL plasma/mL tissue/s (range, 2.1-29.9). Notably, the median tumor CHO uptake values in stage IV metastatic disease were higher than that of stage II (Fig. 3; Table 1).

CHO uptake in normal tissues. Imaging variables derived from normal breast tissue (contralateral normal breast in the case of primary breast cancers) or normal lung were found to be low compared with tumor. Compared with tumor, median Ki and $SUV_{60,av}$ were ~10-fold lower in normal breast (median

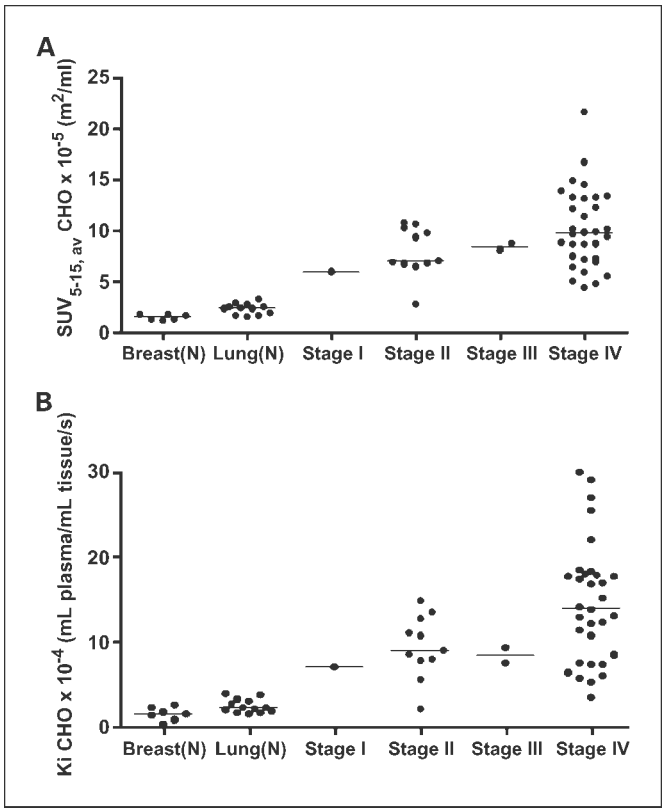

Fig. 3. *A,* CHO $SUV_{5\text{-}15,av}$ in various American Joint Committee on Cancer stages of breast cancer and normal (N) tissues. *B,* Ki CHO of same tumors and normal tissues.

Ki = 1.4×10^{-4}, 95% confidence interval = 6.9×10^{-5} to 2.2×10^{-5} mL plasma/mL tissue/s; median $SUV_{60,av} = 1.2 \times 10^{-5}$, 95% confidence interval 0.6×10^{-5} to 1.7×10^{-5} m^2/mL) and normal lung (Ki = 3.1×10^{-4}, 95% confidence interval = 1.8×10^{-4} to 4.4×10^{-4} mL plasma/mL tissue/s; $SUV_{60,av} = 1.8 \times 10^{-5}$, 95% confidence interval = 1.3×10^{-5} to 2.5×10^{-5} m^2/mL).

Association of CHO PET parameters with tumor grade and size. Tumor grade and size are well-known prognostic indicators (35, 36). There was a poor association between PET variables and tumor size (Table 2). This may be due to the fact that tumor size per se is not a measure of malignant transformation and progression. Analysis of maximal voxel activity rather than average tumor activity seemed to improve the association of PET variables with tumor size, but the correlation coefficient was still below 0.5. Tumor grade was available for all primary cases and two metastatic cases. $SUV_{60,max}$ correlated well with histologic grade of primary tumors (Table 2; $P = 0.005$, $r = 0.70$, Spearman's test), and grade also correlated well with imaging variables when primary and metastatic tumors were combined (the grade of the metastatic lesion was by definition the same as the original primary tumor); Ki had the best comparative correlation ($P = 0.0002$, $r = 0.53$, Spearman's test; Table 2). Overall, the association of imaging variables with grade increased in the order $SUV_{5\text{-}15} < SUV_{60,av} < SUV_{60,max} <$ Ki. We could not find any association of CHO PET variables and ER, PR, HER-2, or pathologically involved nodes (Table 2), a fact that is largely due to the patient inclusion criteria for this study. Ki-67 did not correlate with CHO uptake variables.

Discussion

To our knowledge, this is the first report describing the use of CHO PET in breast cancer patients. Choline metabolism is elevated in the majority of tumors and accounts for increased phospholipid synthesis required for cell membrane turnover (37). In mammary epithelial cells, the increased intracellular phosphocholine levels is associated with malignancy, increasing with transformation and progression (17). The elevated phosphocholine levels in breast cancer cells may be due to elevated choline kinase-α expression (18, 38). Choline kinase-α has been identified as an oncogenic protein and may act in the G_1-S transition to promote cell division. The choline kinase-α–regulated genes that affect G_1-S transition have been reported recently (39). Increased choline metabolism has also been shown to be regulated by the growth factor receptor–MAPK pathway (17, 21, 22, 40), a pathway that is thought to play a central role in resistance to endocrine therapy (4, 6, 11). From these *in vitro* studies and by analogy to studies of choline kinase-α in biopsies from lung cancer patients (25), phosphorylation of choline to phosphocholine may have prognostic value in ER-positive breast cancer patients. To date, CHO PET has been explored largely in prostate cancer imaging (16, 41–43). This study investigates CHO PET imaging in breast cancer.

Median CHO uptake was ~10-fold lower in normal breast and lung tissues compared with tumors and was higher in the more aggressive stage IV tumors compared with stage II tumors; we did not have enough patients in the other categories to make a comparison for all patients. This finding is in keeping with the *in vitro* findings of Aboagye and Bhujwalla, which showed elevated phosphocholine levels with transformation and progression (17). The low background and high signal-to-noise contrast suggests that CHO may be a useful imaging probe for breast cancer. At this stage, we are unable to report the relevance of CHO uptake to overall survival. Of note, patients with stage IV breast cancer showed a large range of uptake values. Although we were careful in selecting patients, this finding may be due in part to the confounding effect of previous treatment (as in metastatic cases) and may not completely reflect CHO uptake in *de novo* metastases. Regarding its sensitivity for routine diagnosis of cancer, CHO-PET did not detect two target lesions, one primary untreated lobular cancer (3 cm) and one (2 cm) metastatic lung lesion. These two lesions were seen clearly on magnetic resonance imaging and computed tomography, respectively. The lung lesion was located at the base of the lung and therefore subject to continuous respiratory movements, which may be the reason that it was not visualized. Other nontarget lesions (<2 cm) were not detected by CHO PET presumably because of their small size. This will suggest that the technique may be best used in conjunction with other imaging technologies, such as computed tomography.

We assessed a number of semiquantitative and fully quantitative CHO PET variables in this setting. SUV did not change significantly between the early imaging time point (5-15 minutes) and late imaging time point (60 minutes) despite the increased proportion of plasma [^{11}C]betaine levels over time (data not shown). We used grade as the gold standard for comparison of imaging variables. Of note, the CHO uptake was largely similar in different tumors within the same patient (by definition, same grade); although in few patients

differences were seen between the primary tumor and involved axillary lymph node(s) consistent with clonal evolution. With respect to grade, $SUV_{60,max}$ was the best imaging variable in primary tumors. For all tumors combined, the association of imaging variables with grade increased in the order $SUV_{5\text{-}15} < SUV_{60,av} < SUV_{60,max} <$ Ki. The fully quantitative estimate, Ki, was expected to be robust because it describes better the conversion of CHO to the intracellular metabolite [^{11}C]phosphocholine in tumor without contribution by the metabolite [^{11}C]betaine. Interestingly, although detailed kinetic modeling may theoretically better reflect tumor properties, the differences in correlation values with grade were not markedly better compared with SUV measures. No correlation with ER, PR, HER-2, or pathologically involved nodes was found; a fact that may be largely due to the selection of ER-positive cases. The absence of a correlation with Ki-67 (primary cases) is interesting and suggests that CHO uptake does not reflect proliferation.

Further to its prognostic value, CHO PET may also be useful as a pharmacodynamic end point for clinical evaluation of choline kinase-α inhibitors, which are currently in preclinical development (44–46), and potentially drugs that act on the MAPK pathway (21). In this context, a correlation between expression of choline kinase in the breast cancer specimens and the PET outcome would greatly improve the understanding of the findings and provide further support to the potential use as a pharmacodynamic noninvasive tool. Furthermore, it will be interesting to assess whether semiquantitative variables are still useful for monitoring drug response because the therapeutics may themselves alter the systemic metabolism of CHO. Two areas that need exploring further are application of this technology to tumors smaller than 2 cm in size to gain an improved understanding of sensitivity and specificity of these radiotracers and application in bone and liver metastases. These data have broad prognostic implications for use of PET scanning in breast cancer to visualize tumor biology *in vivo*. In conclusion, CHO showed good uptake in most breast cancers and merits further investigation as a breast cancer imaging agent.

Disclosure of Potential Conflicts of Interest

No potential conflicts of interest were disclosed.

Acknowledgments

We thank Sian Thomas and Helena Marconell for help in recruiting patients for this study and all the chemists and radiographers from GE-IMANET for their help in radiotracer production and PET scanning.

References

1. Coombes RC, Hall E, Gibson LJ, et al. A randomized trial of exemestane after two to three years of tamoxifen therapy in postmenopausal women with primary breast cancer. N Engl J Med 2004;350:1081–92.
2. Baum M, Buzdar A, Cuzick J, et al. Anastrozole alone or in combination with tamoxifen versus tamoxifen alone for adjuvant treatment of postmenopausal women with early-stage breast cancer: results of the ATAC (Arimidex, Tamoxifen Alone or in Combination) trial efficacy and safety update analyses. Cancer 2003; 98:1802–10.
3. Ali S, Coombes RC. Endocrine-responsive breast cancer and strategies for combating resistance. Nat Rev Cancer 2002;2:101–12.
4. Thomas RS, Sarwar N, Phoenix F, Coombes RC, Ali S. Phosphorylation at serines 104 and 106 by Erk1/2 MAPK is important for estrogen receptor-α activity. J Mol Endocrinol 2008;40:173–84.
5. Adeyinka A, Nui Y, Cherlet T, et al. Activated mitogen-activated protein kinase expression during human breast tumorigenesis and breast cancer progression. Clin Cancer Res 2002;8: 1747–53.
6. Santen RJ, Song RX, Zhang Z, et al. Long-term estradiol deprivation in breast cancer cells upregulates growth factor signaling and enhances estrogen sensitivity. Endocr Relat Cancer 2005; 12 Suppl 1:S61–73.
7. Sarwar N, Kim JS, Jiang J, et al. Phosphorylation of ERα at serine 118 in primary breast cancer and in tamoxifen-resistant tumours is indicative of a complex role for ERα phosphorylation in breast cancer progression. Endocr Relat Cancer 2006;13:851–61.
8. Kato S, Endoh H, Masuhiro Y, et al. Activation of the estrogen receptor through phosphorylation by mitogen-activated protein kinase. Science 1995;270:1491–4.
9. Bunone G, Briand PA, Miksicek RJ, Picard D. Activation of the unliganded estrogen receptor by EGF involves the MAP kinase pathway and direct phosphorylation. EMBO J 1996;15: 2174–83.
10. Sivaraman VS, Wang H, Nuovo GJ, Malbon CC. Hyperexpression of mitogen-activated protein kinase in human breast cancer. J Clin Invest 1997;99:1478–83.
11. Gee JM, Robertson JF, Ellis IO. Nicholson RI Phosphorylation of ERK1/2 mitogen-activated protein kinase is associated with poor response to anti-hormonal therapy and decreased patient survival in clinical breast cancer. Int J Cancer 2001;95:247–54.
12. Kelloff GJ, Hoffman JM, Johnson B, et al. Progress and promise of FDG-PET imaging for cancer patient management and oncologic drug development. Clin Cancer Res 2005;11: 2785–808.
13. Rosen EL, Eubank WB, Mankoff DA. FDG PET, PET/CT, and breast cancer imaging. Radiographics 2007;27 Suppl 1:S215–29.
14. Kenny LM, Vigushin DM, Al-Nahhas A, et al. Quantification of cellular proliferation in tumor and normal tissues of patients with breast cancer by [18F]fluorothymidine-positron emission tomography imaging: evaluation of analytical methods. Cancer Res 2005;65:10104–12.
15. Shields AF, Grierson JR, Dohmen BM, et al. Imaging proliferation *in vivo* with [F-18]FLT and positron emission tomography. Nat Med 1998;4: 1334–6.
16. Hara T, Kosaka N, Kishi H. PET imaging of prostate cancer using carbon-11-choline. J Nucl Med 1998;39:990–5.
17. Aboagye EO, Bhujwalla ZM. Malignant transformation alters membrane choline phospholipid metabolism of human mammary epithelial cells. Cancer Res 1999;59:80–4.
18. Glunde K, Jie C, Bhujwalla ZM. Molecular causes of the aberrant choline phospholipid metabolism in breast cancer. Cancer Res 2004; 64:4270–6.
19. Ramirez de Molina A, Banez-Coronel M, Gutierrez R, et al. Choline kinase activation is a critical requirement for the proliferation of primary human mammary epithelial cells and breast tumor progression. Cancer Res 2004;64:6732–9.
20. Choi MG, Park TS, Carman GM. Phosphorylation of Saccharomyces cerevisiae CTP synthetase at Ser424 by protein kinases A and C regulates phosphatidylcholine synthesis by the CDP-choline pathway. J Biol Chem 2003;278: 23610–6.
21. Liu D, Hutchinson OC, Osman S, et al. Use of radiolabelled choline as a pharmacodynamic marker for the signal transduction inhibitor geldanamycin. Br J Cancer 2002;87: 783–9.
22. Ratnam S, Kent C. Early increase in choline kinase activity upon induction of the H-ras oncogene in mouse fibroblast cell lines. Arch Biochem Biophys 1995;323:313–22.
23. Hernandez-Alcoceba R, Saniger L, Campos J, et al. Choline kinase inhibitors as a novel approach for antiproliferative drug design. Oncogene 1997;15:2289–301.
24. Yu Y, Sreenivas A, Ostrander DB, Carman GM. Phosphorylation of Saccharomyces cerevisiae choline kinase on Ser30 and Ser85 by protein kinase A regulates phosphatidylcholine synthesis by the CDP-choline pathway. J Biol Chem 2002; 277:34978–86.
25. Ramirez de Molina A, Sarmentero-Estrada J, Belda-Iniesta C, et al. Expression of choline kinase α to predict outcome in patients with early-stage non-small-cell lung cancer: a retrospective study. Lancet Oncol 2007;8: 889–97.
26. Pascali CAB, Itawa R, Cambiè M, Bombardieri E. [11C]Methylation on a C18 Sep-Pak cartridge: a convenient way to produce [N-methyl-11C] choline. J Labelled Compds Radiopharm 2000; 43:195–203.

27. Hara T, Yuasa M. Automated synthesis of [^{11}C] choline, a positron-emitting tracer for tumor imaging. Appl Radiat Isot 1999;50:531–3.

28. Lucignani G, Paganelli G, Bombardieri E. The use of standardized uptake values for assessing FDG uptake with PET in oncology: a clinical perspective. Nucl Med Commun 2004;25:651–6.

29. Hara T, Kosaka N, Shinoura N, Kondo T. PET imaging of brain tumor with [methyl-11C]choline. J Nucl Med 1997;38:842–7.

30. Mankoff DA, Shields AF, Graham MM, Link JM, Krohn KA. A graphical analysis method to estimate blood-to-tissue transfer constants for tracers with labeled metabolites. J Nucl Med 1996;37:2049–57.

31. Patlak CS, Blasberg RG. Graphical evaluation of blood-to-brain transfer constants from multiple-time uptake data. Generalizations. J Cereb Blood Flow Metab 1985;5:584–90.

32. Elston CW, Ellis IO. Pathological prognostic factors in breast cancer: I. The value of histologic grade in breast cancer: experience from a large study with long-term follow-up. Histopathology 1991;19:403–10.

33. McCarty KS, Jr., Miller LS, Cox EB, Konrath J, McCarty KS, Sr. Estrogen receptor analyses. Correlation of biochemical and immunohistochemical methods using monoclonal antireceptor antibodies. Arch Pathol Lab Med 1985;109:716–21.

34. Millis RR, Barnes DM, Lampejo OT, Egan MK, Smith P. Tumour grade does not change between primary and recurrent mammary carcinoma. Eur J Cancer 1998;34:548–53.

35. Dunnwald LK, Rossing MA, Li CI. Hormone receptor status, tumor characteristics, and prognosis: a prospective cohort of breast cancer patients. Breast Cancer Res 2007;9:R6.

36. D'Eredita G, Giardina C, Martellotta M, Natale T, Ferrarese F. Prognostic factors in breast cancer: the predictive value of the Nottingham Prognostic Index in patients with a long-term follow-up that were treated in a single institution. Eur J Cancer 2001;37:591–6.

37. Ramirez de Molina A, Rodriguez-Gonzalez A, Gutierrez R, et al. Overexpression of choline kinase is a frequent feature in human tumor-derived cell lines and in lung, prostate, and colorectal human cancers. Biochem Biophys Res Commun 2002;296:580–3.

38. Katz-Brull R, Margalit R, Bendel P, Degani H. Choline metabolism in breast cancer; 2H-, 13C- and 31P-NMR studies of cells and tumors. Magma 1998;6:44–52.

39. Ramirez de Molina A, Gallego-Ortega D, Sarmentero-Estrada J, et al. Choline kinase as a link connecting phospholipid metabolism and cell cycle regulation: implications in cancer therapy. Int J Biochem Cell Biol 2008;40:1753–63.

40. Hernandez-Alcoceba R, Fernandez F, Lacal JC. *In vivo* antitumor activity of choline kinase inhibitors: a novel target for anticancer drug discovery. Cancer Res 1999;59:3112–8.

41. Reske SN. [11C]Choline uptake with PET/CT for the initial diagnosis of prostate cancer: relation to PSA levels, tumour stage and anti-androgenic therapy. Eur J Nucl Med Mol Imaging 2008;35:1740–1.

42. Reske SN, Blumstein NM, Glatting G. [11C] choline PET/CT imaging in occult local relapse of prostate cancer after radical prostatectomy. Eur J Nucl Med Mol Imaging 2008;35:9–17.

43. Rinnab L, Simon J, Hautmann RE, et al. [(11)C] choline PET/CT in prostate cancer patients with biochemical recurrence after radical prostatectomy. World J Urol 2009.

44. Al-Saffar NM, Troy H, Ramirez de Molina A, et al. Noninvasive magnetic resonance spectroscopic pharmacodynamic markers of the choline kinase inhibitor MN58b in human carcinoma models. Cancer Res 2006;66:427–34.

45. Conejo-Garcia A, Banez-Coronel M, Sanchez-Martin RM, et al. Influence of the linker in bispyridium compounds on the inhibition of human choline kinase. J Med Chem 2004;47:5433–40.

46. Campos J, Nunez MC, Conejo-Garcia A, et al. QSAR-derived choline kinase inhibitors: how rational can antiproliferative drug design be? Curr Med Chem 2003;10:1095–112.